Colloids and Surfaces A: Physicochemical and Engineering Aspects 705 (2025) 135542

Contents lists available at ScienceDirect

Colloids and Surfaces A: Physicochemical and Engineering Aspects

journal homepage: www.elsevier.com/locate/colsurfa

Carbon nanofiber orientation influences bacterial adhesion under flow conditions

Julia Schulte-Hermann [a], Hagen Rießland [a], Stefan Hengsbach [a,b], Jan G. Korvink [a], Neil MacKinnon [a,*], Monsur Islam [c,*]

[a] Institute of Microstructure Technology (IMT), Karlsruhe Institute of Technology, Hermann-von-Helmholtz-Platz 1, Eggenstein-Leopoldshafen, 76344, Germany
[b] Karlsruhe Nano Micro Facility KNMFi, Karlsruhe Institute of Technology, Hermann-von-Helmholtz-Platz 1, Eggenstein-Leopoldshafen, 76344, Germany
[c] IMDEA Materials Institute, Tecnogetafe, Calle Eric Kandel 2, Getafe, Madrid, 28906, Spain

GRAPHICAL ABSTRACT

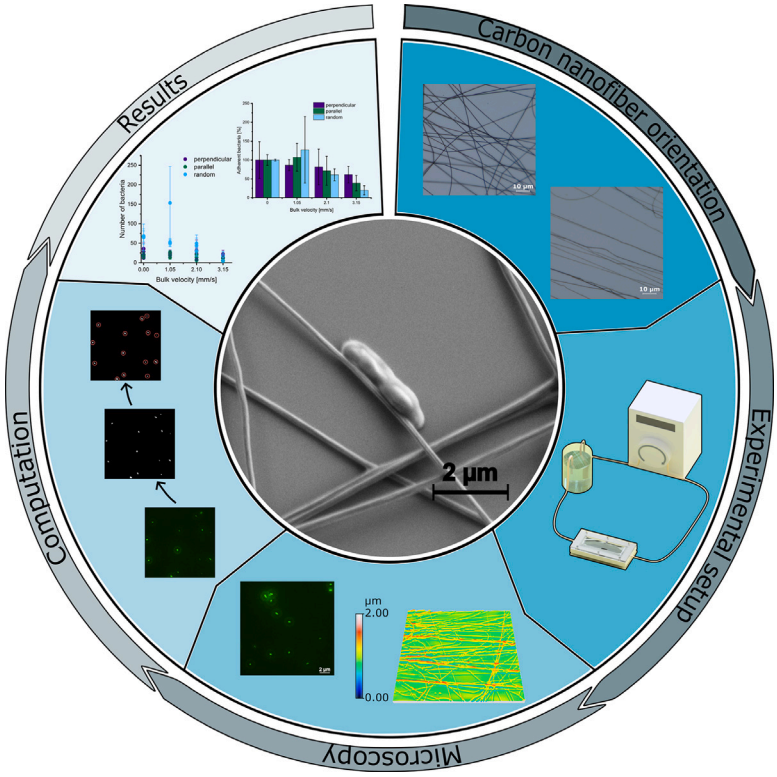

ARTICLE INFO

MSC:
0000

ABSTRACT

Biosensing methods continue to increase in complexity, and together with growing interest in living materials, new options for fixing bacteria under flow conditions are needed. Current methods of cell fixation consist of

* Corresponding authors.
E-mail addresses: julia.schulte-hermann@kit.edu (J. Schulte-Hermann), neil.mackinnon@kit.edu (N. MacKinnon), monsur.islam@imdea.org (M. Islam).

https://doi.org/10.1016/j.colsurfa.2024.135542
Received 12 August 2024; Received in revised form 20 September 2024; Accepted 9 October 2024
Available online 18 October 2024

1111

Keywords:
Carbon nanofiber
Bacteria fixation

microfluidic cell trapping, dielectrophoretic immobilization, chemical fixation, or cell encapsulation. However, these methods come with disadvantages, such as chemical alteration, isolation, or exposure to high shear forces. In this work we present electrospun carbon nanofibers as a new cell scaffold material, and explored the potential of this material for bacterial adhesion under normal flow conditions. To characterize immobilization, model organisms *E. coli* were introduced into carbon nanofiber samples, and after an incubation period, perfusion at different flow speeds was applied. Adhesion was quantified by counting the number of bacteria remaining on the scaffold after a fixed period of flow exposure. The fibers were additionally characterized for their wettability and surface roughness, properties expected to influence adhesion. It was observed that a larger fraction of bacteria remained on the scaffold as flow rates increased in comparison with surfaces without the scaffold. Thus, electrospun carbon nanofibers provide an interesting approach of bacterial fixation given their biocompatibility and tune-able properties (*e.g.* electrical conductivity and fiber diameter), opening a variety of applications and enabling tailored scaffolds optimized for a variety of processes and bacteria strains.

1. Introduction

The past decade has witnessed a substantial interest in using living bacteria in functional assays, owning to their adaptive and autonomous characteristics. Examples of applications include biosensing [1–4], material synthesis [5–7], and energy production [8,9]. These often require the bacteria in conjunction with an abiotic substrate or scaffold. Thus, bacterial fixation or adhesion is an important criterion for these applications. For example, biohybrid living photoelectric cells require a strong adhesion between the bacterium and an electrode surface to enable easier and more efficient electron exchange among them for energy storage purposes.

Common current approaches for bacterial immobilization include chemical fixation, microfluidic traps [10–12], gel matrices [13,14], trapping through antibodies [15], fiber trapping [16–18], and dielectrophoretic trapping [19]. However, these approaches feature several disadvantages.

Chemical fixation with formaldehyde or similar analytes alters the cell integrity and dimensions, and reduces the concentration of fluorescent proteins, which are important in applications such as biosensing [20].

Microfluidic traps are mainly used for minimally invasive, targeted single-cell trapping. Microstructures are used to fixate cells in a predetermined position. These structures can be wells with inverse-tapered walls [10], wells with slanted side walls [11], or column structures [12]. A detailed overview of hydrodynamic trapping systems is given by Luan et al. [21]. A similar approach is provided by trapping through the use of membranes [22]. However, depending on the flow field that the cells experience, they are exposed to non-negligible shear forces [23], and clogging of the structures or membrane can result.

Cell encapsulation within gel matrices, such as hydrogels or polymers [13,14], while avoiding shear forces, reduces a cell's reaction time to analytes, and decreases potential adsorption of the analytes by the gel material [3]. Flickinger et al. [24] managed to increase the reaction time of gel-entrapped bacteria by printing bacteria as a nano-porous gel film. The integration of antibodies into a gel matrix, facilitating cell adhesion, increases the reaction time of whole-cell biosensors [15]. However, hydrogel trapping is sensitive to flow conditions and non-constant flows [13].

Encapsulating bacteria using an electrospun polymer and bacterial solution, under the correct conditions [16,18], enables bacteria to be entrapped within the fiber itself. A similar fiber-based approach is the treatment of fibers, such as cotton, polyester, viscose rayon, and silk, with a crosslinking agent for fixating the bacteria [17].

Unfortunately, a perfect matrix has not been identified, as these methods come with drawbacks: altered cell integrity, exposure to shear force stress, decrease in response time, flow sensitivity, or complicated manufacturing or coating processes.

In this paper, we postulate electrospun carbon nanofibers as a matrix material for bacterial fixation for flow conditions. Carbon is a highly biocompatible material [25–28] and is widely used for various biological applications [27,29–31]. Furthermore, carbon nanofibers feature good electrical conductivity and tunable porous microstructures, making them suitable electrode materials in applications such as sensors and energy devices [32–35]. Carbon nanofibers have a high potential to integrate with living cells, particularly bacteria, to develop biohybrid living systems and further enhance their performances in sensing or energy storage [36]. However, towards such development, it is essential to consider substrate adhesion.

Here, we study bacterial adhesion to electrospun carbon nanofibers applied on a silicon substrate under varying flow conditions. The adhesion is compared with a blank silicon substrate, commonly used in MEMS-based devices, as well with carbon film applied on silicon. Furthermore, adhesion is also evaluated for the effect of carbon nanofiber orientation, and correlated with the surface properties of carbon nanofibers.

2. Materials and methods

2.1. Fabrication of carbon nanofibers

The fabrication process of carbon nanofibers is illustrated in Fig. 1, which involves the electrospinning of polyacrylonitrile (PAN) and subsequent pyrolysis. To facilitate the electrospinning, PAN was first dissolved in N,N-dimethylformamide (DMF; Catalog number: 1.03053.2511, VWR, Germany) to yield a concentration of 10% (wt.%). The PAN/DMF solution was electrospun using the following parameters: voltage = 10 kV, spinneret to collector distance = 10 cm, solution flow rate = 10 μL min^{-1}. Electrospun fibers were collected on a silicon (Si) substrate, featuring an area of 1 cm^2. Silicon was chosen as the base material due to its heat resistance, making it suitable as a carrier substrate for pyrolysis, and the adhesion of carbon nanofibers to the material during exposure to liquids. Typically, this configuration of electrospinning resulted in random fiber orientation. To obtain aligned fibers, the as-spun fibers were manually pulled on Si substrates. Upon electrospinning, the fibers were stabilized on a hot plate at 200 °C for 2 h to promote cross-linking of the polymer. The electrospun PAN fibers were next carbonized in a horizontal tube furnace (Nabertherm, Germany) at 900 °C for 2 h in a constant nitrogen gas flow (80 L h^{-1}) condition, as typically used for the carbonization of organic precursors [37,38]. Fig. 1 presents examples of randomly oriented carbon nanofibers and aligned carbon nanofibers. The flow-through experiments used three different configurations of these carbon nanofibers, which included (i) the randomly oriented carbon nanofibers, (ii) aligned carbon nanofibers with the orientation parallel to the flow, and (iii) aligned carbon nanofibers with orientation perpendicular to the flow. For comparison with the carbon nanofiber samples, we also prepared a planar carbon film through dropcasting of PAN/DMF solution followed by carbonization. To determine the influence of the silicon on the measurements, bare silicon was investigated as well.

2.2. Material characterization

Surface properties, such as wettability and surface roughness, strongly influence bacteria adhesion on surfaces [39,40]. The wettability

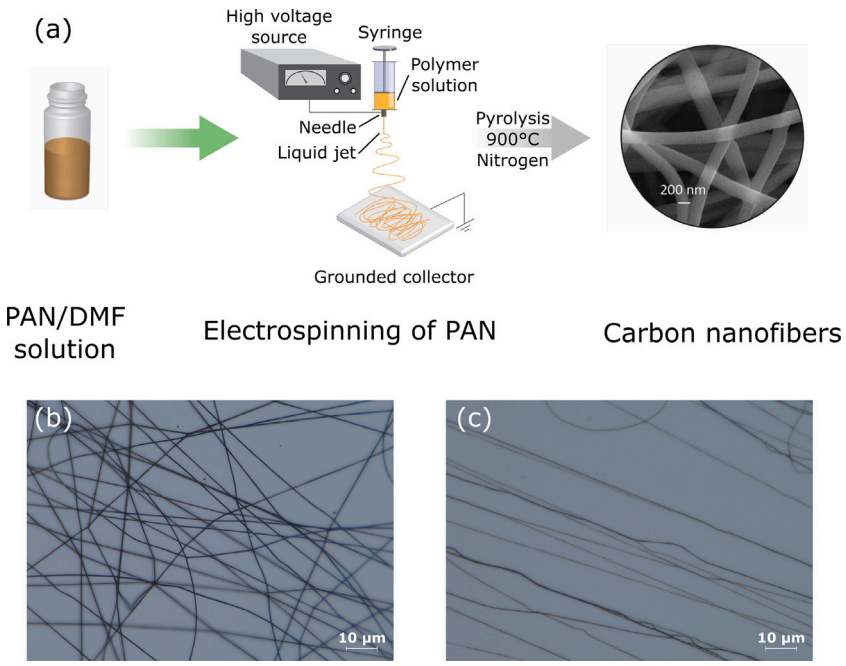

Fig. 1. (a) Fabrication process of carbon nanofibers on silicon. (b) Randomly orientated carbon nanofibers. (c) Aligned carbon nanofibers.

of the investigated materials was characterized through contact angle measurements using an OCA20 from DataPhysics. For the measurement, a droplet of 1 µL distilled water was formed at the tip of a syringe. The syringe tip was then lowered until the droplet touched the surface of the material, and the droplet was released from the syringe by lifting the syringe. A picture of the droplet on the surface was captured. The contact angle of the water droplet was determined with the contact angle plugin of ImageJ [41]. Contact angles of $\theta > 90°$ indicate hydrophobicity and contact angles of $\theta < 90°$ show hydrophilicity [42].

We measured the surface roughness of our samples using confocal scanning microscopy (MarSurf Expert, Mahr). The optical system used for the microscopy featured a lens of 100 magnification, a free working distance of 1 mm, a numerical aperture of 0.8, and a visual field of 160 by 160 µm. Confocal scanning microscopy is based on dynamic focusing and a focus detection technique, meaning only image information is recorded which is in the focus point. To generate surface topography images, the substrate or lens is adjusted vertically, and the microscope detects the focused parts of the substrate. A detailed description of the working principle of confocal scanning microscopy has been given by Udupa et al. [43] With the generated topography maps of the samples, the arithmetical mean height (Sa) and root square mean height (Sq) were calculated using Eq. (1).

$$Sa = \frac{1}{A}\iint_A |z(x,y)|\mathrm{d}x\mathrm{d}y \tag{1a}$$

$$Sq = \sqrt{\frac{1}{A}\iint_A z^2(x,y)\mathrm{d}x\mathrm{d}y} \tag{1b}$$

The arithmetical mean height (Sa) is the difference in height of each point compared to the arithmetical mean of the surface. It is used to evaluate surface roughness [44]. The root square mean height (Sq) is equivalent to the standard deviation of heights [45]. For each sample type, we evaluated an area of 100 µm × 100 µm.

2.3. Bacteria cultivation

A BL21(DE3) *Escherichia coli* strain, with the pET_ST-eGFP-His plasmide producing green fluorescent protein (GFP) with an emission wavelength of 516 nm to 556 nm when exposed to isopropyl *β*-D-1-thiogalactopyranoside (IPTG), was selected as a model organism to investigate bacterial adhesion [46]. Advantages of using *E. coli* include relatively simple cultivation, their accessibility, and well-known behavior and properties. The fluorescence enables bacteria visibility of samples under a fluorescence microscope. To ensure comparability and reproducibility, a liquid culture of GFP emitting *E. coli* was incubated in 20 mL LB media, 0.269 26 mmol L^{-1} ampicillin sodium salt, and 100 µmol IPTG for 18 h in an incubator at 37 °C. Cryostocks were created from the incubated liquid culture by centrifuging 10 mL at 4000rev min^{-1} for 10 min. The excess liquid was removed, and the bacteria were resuspended in 10 mL phosphate-buffered saline (PBS). Then, the centrifuging and resuspending steps with PBS were repeated. Before another repetition, the OD_{600} was measured to ensure a high enough bacteria density in the PBS. Afterward, the solution was centrifuged again at 4000rev min^{-1} for 10 min, the excess liquid was removed, and the cells were resuspended with 5 mL LB media. 30 cryostocks were created from the solution by adding 23.25 µL of 80% glycerol, 26.75 µL H_2O and 50 µL of the prepared bacteria solution in a micro tube. Each tube is vortexed and then placed in a −20 °C freezer. One cryostock was utilized per adhesion test. The cryostock was defrosted by placing it in a 8 °C fridge for 20 min before centrifugation at 5000rev min^{-1} for 10 min. Afterward, the excess liquid was removed, and the bacteria were resuspended in 10 mL of LB media. The next step was the detection of the optical density, OD_{600}, to estimate the amount of required bacteria culture to achieve an OD_{600} of 0.005 in 20 mL LB media. The fresh LB media, bacteria culture at 37 °C, 20 µL ampicillin sodium salt, and 100 µmol IPTG were mixed.

2.4. Sample preparation

The substrate samples were placed in a Petri dish and exposed to 20 mL of the prepared bacteria culture with an OD_{600} of 0.005. For cell growth, the samples were incubated at 37 °C for two hours in the bacteria culture. After incubation, the samples were stored in PBS for bacterial preservation. PBS is qualified for bacteria preservation [47, 48] as it prevents deleterious effects due to osmosis, *e.g.* cell rupturing.

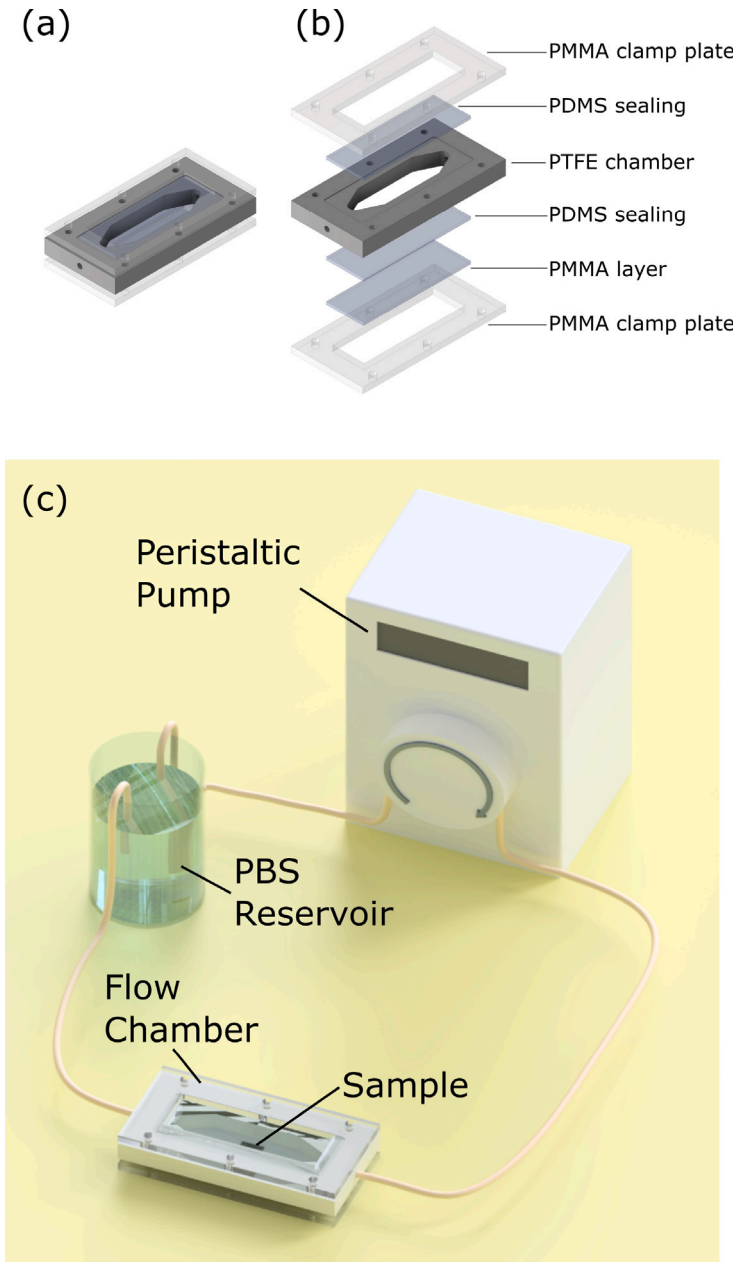

Fig. 2. Flow chamber. (a) Assembled view. (b) Exploded view. (c) Experimental setup of adhesion assay.

2.5. Experimental setup

The flow chamber for conducting the adhesion testing is illustrated in Fig. 2. The chamber contained a PTFE main chamber, two PDMS seals on both sides, an additional PMMA slide at the bottom for increased stability, and two PMMA clamp plates on the top and bottom for assembling the flow chamber. The chamber was mounted with screws. The PTFE part was crafted by milling and drilling, the different PMMA parts were fabricated by laser cutting, and the PDMS parts were cut out of a PDMS layer. The outer dimensions of the assembled chamber are 100 mm × 50 mm × 23 mm. Inside the flow chamber is a flow zone with a length of 37 mm, width of 19 mm and 9 mm height. The flow zone is connected on both ends with triangle shaped filling and draining zones, each with a length of 15 mm and also a height of 9 mm. The chamber was tilted by 7.4° to the flow direction to avoid bubble trapping during the experiments due to the periodic draining and filling with PBS.

The components for the adhesion tests (a peristaltic pump (ISMATEC REGLO ICC), a PBS reservoir, and the flow chamber), were connected via silicone tubing, illustrated in Fig. 2. The bulk velocity in the flow chamber was determined by applying Eq. (2) with the dimensions of the flow chamber and the volumetric flow rate. Since the volumetric flow rate is equal in the flow chamber and the pump, we applied the values of the calibrated pump.

The diameter of the silicone tubing in the peristaltic pump was 3.17 mm and the cross-section of the flow chamber was 171 mm^2.

$$\bar{u} = \frac{\dot{V}}{A_{\text{Chamber}}} \tag{2}$$

2.6. Adhesion tests and evaluation

Our tested bulk velocities are: 0, 1.05, 2.10 and 3.15 $mm\,s^{-1}$. The bulk velocity values are based on flow speeds used for hydrodynamic

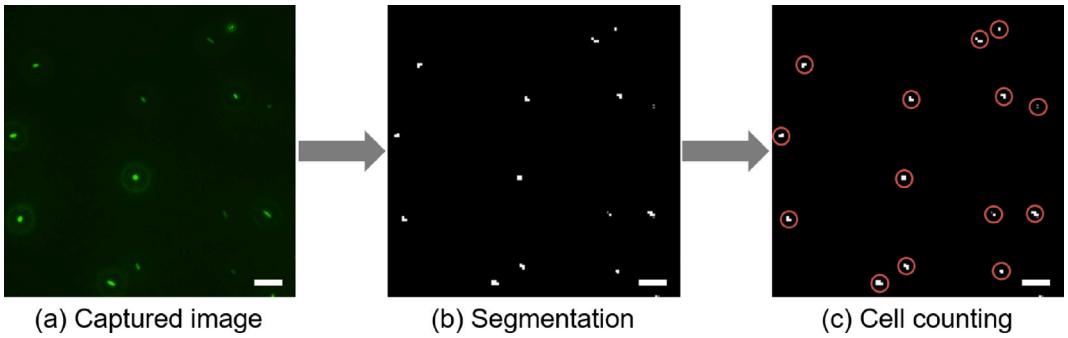

Fig. 3. (a) Microscope image acquisition. (b) Image segmentation using ilastik [50]. (c) Cell counting using a Python-4-implemented watershed algorithm. Scale bar 20 µm in each picture.

cell trapping [21]. While higher values are also applied for cell trapping, the peristaltic pump limited us from testing at higher bulk velocity. Additionally, too high bulk velocities might lead to higher stress and possible cell rupturing. Ishantha Senevirathne et al. [49] investigated the effect of an increase in shear forces on bacteria on nanostructures and found an increase in bactericidal efficacy. For the highest tested bulk velocity in our work, the wall shear force was calculated to be approximately 0.021 Pa, which is significantly lower than the shear forces reported in the literature. The estimated shear force was calculated under the assumed conditions of steady-state incompressible laminar flow with no-slip boundary. Such a small shear force was assumed to exert minimal impact on our experimental setup. However, a detailed study with numerical simulation correlating the experimental findings is needed to fully understand the impact of shear stresses on bacterial adhesion in microfluidic systems.

In our work, three samples per bulk velocity and sample type were tested. The sample was centered in the flow chamber, and the liquid flow was started after sealing the flow chamber. As soon as the chamber was completely filled, a timer was started and the flow speed was held constant for 5 min. Afterwards, the flow chamber was drained and the sample was removed. Each sample was stored for 15 min in formaldehyde after flow exposure to fixate the bacteria, then placed again in PBS and in the dark until examination with a fluorescence microscope. The storage in the dark decreases the decay of the GFP. The fluorescence microscope (Nikon Ti Eclipse) excited GFP with a wavelength range of 464 nm to 499 nm. GFP emits light in the wavelength range of 516 nm to 556 nm. While the bacteria were continuously excited and emitted light, the samples were scanned, and ten images were captured with a magnification of 40x. The images were evaluated by running a segmentation step (software ilastik [50]) to minimize the noise before counting the number of bacteria using a watershed algorithm in Python 3. Fig. 3 visualizes the sample evaluation steps.

2.7. SEM images

SEM images were captured with a Carl Zeiss AG - SUPRA 60VP to visualize bacteria adhesion onto the carbon nanofibers. For comparison, the carbon film and silicon substrates were also investigated. The samples were incubated as described above. Since characterization in an SEM must be carried out under vacuum conditions, the sample must be prepared accordingly without losing its properties. A common option is sputtering the sample with gold. However, to not influence the carbon nanofibers samples, the samples were dried and the acceleration voltage was lowered to 1.5 kV. For the drying process the samples were first dehydrated using ethanol after the incubation period. The first step was placing the samples in a Petri dish filled with 15 mL PBS and incubating them for 2 min on an orbital shaker with 50 rpm. Afterward, the PBS was replaced with 15 mL distilled water, and the samples were shaken again at 50 rpm for 5 min. This step was repeated one more time. The water was then removed, and 15 mL of a 25% ethanol and 75% distilled water mixture was added. This mixture was replaced after 5 min with 15 mL of a 50% ethanol and 50% distilled water mixture. The liquid was substituted with 15 mL of 75% ethanol and 25% distilled water, and the samples were washed at 50 rpm for 5 min. This step was repeated with 15 mL of a mixture of 95% ethanol and 5% distilled water. Afterward, the liquid was removed, and 15 mL of 100% anhydrous ethanol was added to the samples, which were then washed for 5 min at 50rev min^{-1}. This step was repeated two more times. The samples were then dried for 20 min. The last preparation step was placing the samples in 3M™ Novec™ 7100 High-Tech fluid for 2 min followed by a final drying step for 1 min. Due the low viscosity of this fluid the surface tension arises while drying can be decreased significantly. The attributes of this fluid allow fast evaporation. The samples were placed into the SEM for imaging.

3. Results and discussion

3.1. Material characterization

The contact angle of the carbon nanofibers mat exhibited a dependency on fibre orientation. The observed contact angles, summarized in Fig. 4, were 99° ± 5°, 75° ± 4°, 50° ± 1°, and 59° ± 0.5° for the randomly oriented carbon nanofiber, aligned carbon nanofiber, carbon film, and bare silicon samples.

From analysis of the surface topology (Fig. 5), a difference in fiber density was found between the samples with randomly oriented compared to aligned carbon nanofibers. Using an area of 100 µm × 100 µm to calculate the arithmetical mean height, surface roughness was observed to increase: silicon < carbon film < random fibers < aligned fibers (3.7 nm, 6.3 nm, 19 nm, and 140 nm). The increased roughness of the randomly oriented fibers likely stems from the increased fiber density, reflected in the large root mean square height of 180 nm measured for this sample. The fiber density could also explain the relatively large variations in contact angle measurements for these two samples, as a droplet had the possibility to contact the fiber and/or silicon substrate.

3.2. SEM images

Fig. 6 presents the SEM images of adhering *E. coli* on the silicon, carbon film, and randomly oriented carbon nanofiber samples. Given the relatively harsh sample preparation procedure, the SEM images could not be used for any quantitative analysis. For this reason, we were not able to find *E. coli* on the samples with aligned carbon nanofibers. Nevertheless, it could be demonstrated that bacteria do not only adhere to silicon and carbon films, but also to carbon nanofibers (Fig. 6(c)). The average fiber diameter for the randomly orientated carbon nanofibers was 180±30 nm and for the aligned carbon nanofibers 131 ± 30 nm. The significant difference in the diameter of the randomly

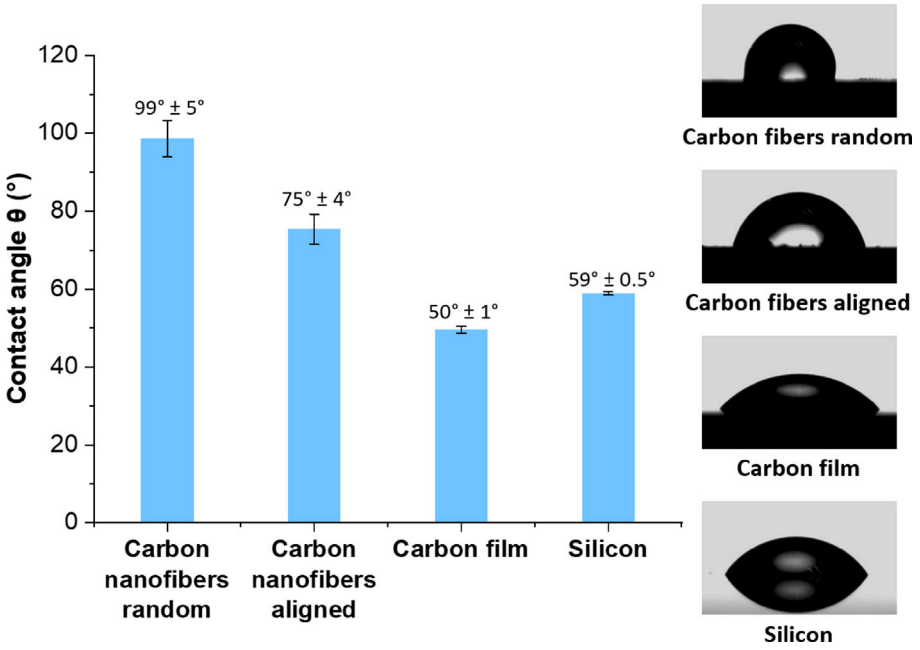

Fig. 4. Contact angle measurements on substrates of randomly oriented carbon nanofibers, aligned carbon nanofibers, carbon film, and silicon.

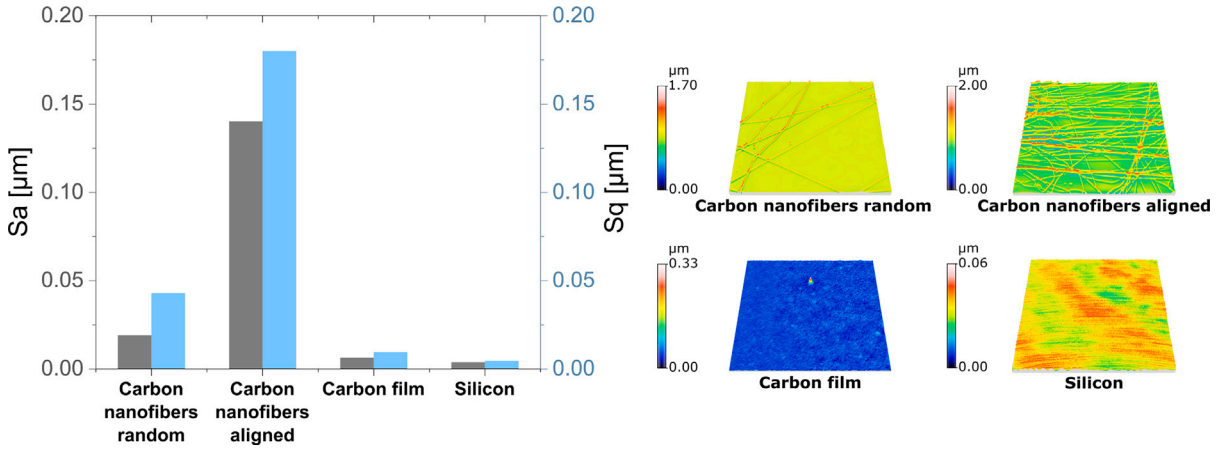

Fig. 5. Surface topography of substrates of randomly oriented carbon nanofibers, aligned carbon nanofibers, carbon film and silicon, over an area of 100 µm×100 µm. The arithmetical mean height (Sa) and root square mean height (Sq) of each sample were calculated.

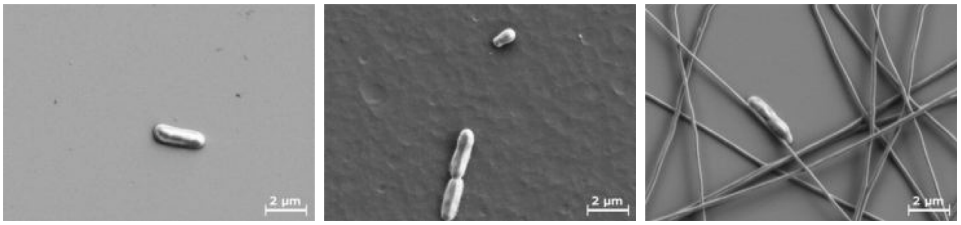

Fig. 6. SEM images of *E. coli* on different substrates. (a) Silicon. (b) Carbon film. (c) Randomly oriented carbon nanofibers.

oriented (M = 180 nm, SD = 29) and aligned fibers (M = 131 nm, SD = 30) was significant, $t(20) = 3.66$, $p = 0.0007$, could be attributed to the manual pulling of the precursor fibers. The manual pulling can cause internal stretching of the polymeric chains, finally leading to decreased fiber diameter, as also observed for electrospun carbon nanofibers obtained on a rotating drum collector [51].

3.3. Adhesion tests

To evaluate the total bacteria amount per sample, the cells were counted over ten captured fluorescence images over different regions of each sample. Each picture covered a surface of 500 µm × 500 µm. Per bulk velocity, three samples were investigated and the collected values

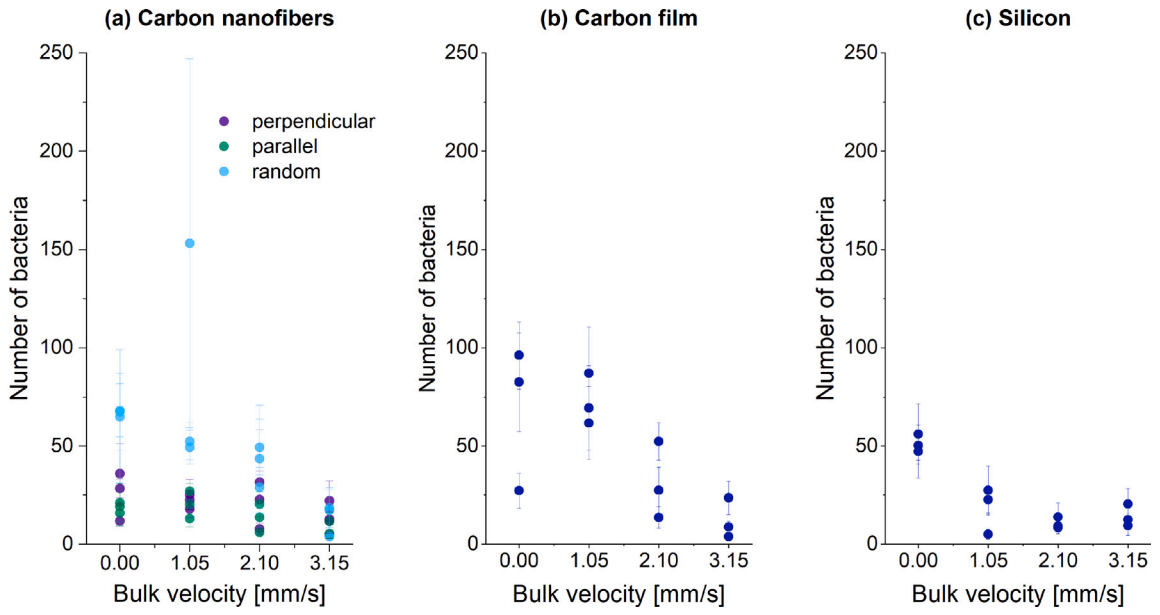

Fig. 7. Number of bacteria vs. bulk velocity for different samples (mean ± standard deviation). (a) Carbon nanofiber orientations. (b) Carbon film. (c) Silicon. Each plotted point is the average over ten images taken in different regions of a single sample. Each substrate was measured in triplicate at each flow rate.

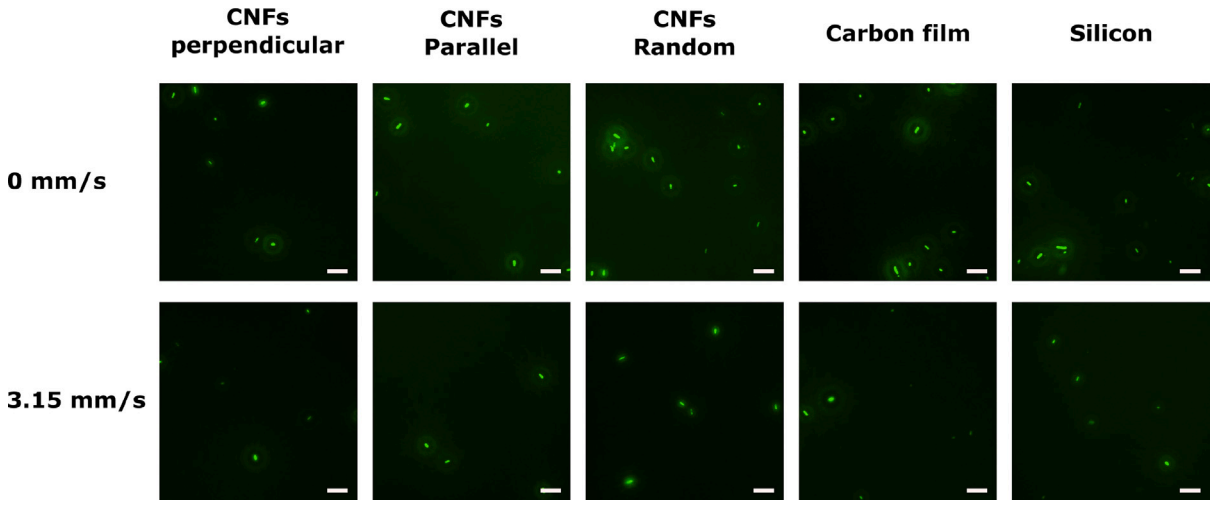

Fig. 8. Exemplary fluorescence images of the different sample types at 0 and $0.315\,\mathrm{mm\,s^{-1}}$. Scale bar $20\,\mu\mathrm{m}$ in each picture.

were averaged. These values are plotted for all sample types in relation to the different flow speeds (Fig. 7).

A trend of decreasing bacteria numbers as the flow rate increased was observed across all sample types. The carbon film had the largest initial number of bacteria, followed by randomly oriented carbon fibers, silicon, and parallel and perpendicular fibers. At the highest bulk velocity tested ($3.15\,\mathrm{mm\,s^{-1}}$), the number of bacteria remaining on the substrates was also observed to be similar across all samples.

Silicon performed the worst in retaining bacteria at the intermediate bulk velocities compared to the carbon substrates.

A one-way ANOVA revealed a statistically significant difference in the mean of the counted bacteria between at least two samples ($F(2,27) = [10,501]$, $p = 0,00042$) of the randomly oriented carbon nanofibers at $1.05\,\mathrm{mm\,s^{-1}}$. A post-hoc Scheffe test revealed, that the sample with an average bacteria count of 153 bacteria is statistically significant different from the other two samples and could be based on the carbon nanofiber density distribution. However, for the three samples of carbon film at $0\,\mathrm{mm\,s^{-1}}$, an ANOVA did show no statistically significant difference between the counted bacteria amounts ($F(2,27) = [2,8301]$, $p = 0,077$). Still for the sample of an lower average of 29 counted bacteria compared to the 43 and 49 counted bacteria, the manufacturing could have contributed. It was observed that the precursor PAN fibers and PAN film were not always evenly distributed before pyrolysis.

To show a significant difference between the groups, a Student's t-test was conducted for the bacterial adhesion at $0\,\mathrm{mm\,s^{-1}}$, by comparing the means of the different samples. The resulting values can be found in Table 1. The test revealed that there is a statistically significant difference between most of the samples, aside from that resulting from differences among perpendicular to parallel oriented carbon nanofibers. This was expected due to the samples being fabricated the same way and not experiencing a difference due flow exposure at $0\,\mathrm{mm\,s^{-1}}$. Further, there was also no statistically significant difference between the initial bacterial adhesion to random oriented carbon nanofibers and carbon film.

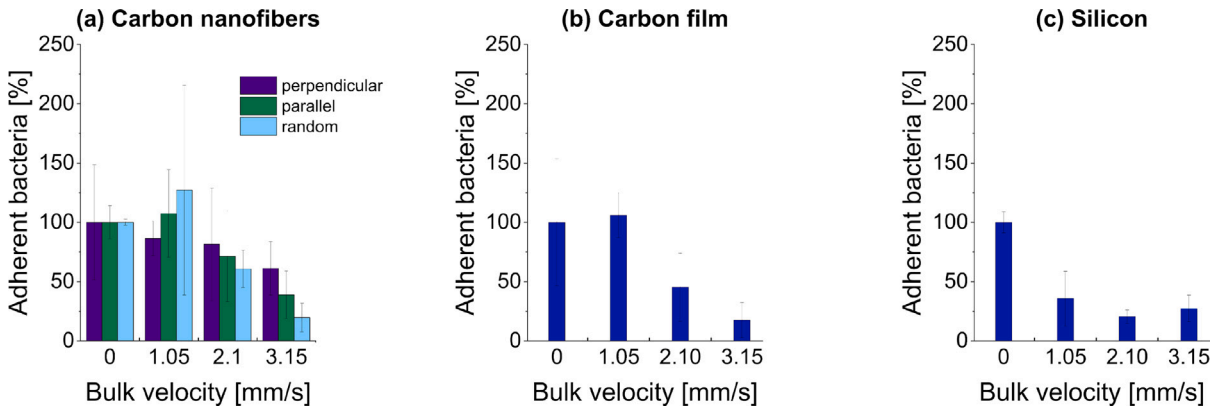

Fig. 9. Bacterium adhesion count (percentage) vs. bulk velocity of the different samples. (a) Different carbon nanofiber orientations. (b) Carbon film. (c) Silicon.

Table 1
Student's t-test results for the initial adhering bacteria at a bulk velocity of $0\,mm\,s^{-1}$ of the different samples for $\alpha = 0.05$. For p-values smaller than α, there is a statistically significant difference. Values with blue background show a statistically significant difference, whereas values with gray background do not.

		Parallel oriented carbon nanofibers M = 18.63 SD = 6.92	Perpendicular oriented carbon nanofibers M = 25.3 SD = 150.75	Carbon film M = 68.63 SD = 1340.00	Silicon M = 51.17 SD = 20.81
Random oriented carbon nanofibers	M = 66.83 SD = 2.89	p = 6*e-6	p = 0.002	p = 0.4	p = 0.003
Parallel oriented carbon nanofibers	M = 18.63 SD = 6.92		p = 0.2	p = 0.04	p = 0.0002
Perpendicular oriented carbon nanofibers	M = 25.3 SD = 150.75			p = 0.04	p = 0.01
Carbon film	M = 68.63 SD = 1340.00				p = 0.2

An alternate view of the data is to estimate the relative bacteria loss as a function of flow rate for the various samples tested by normalizing the number of bacteria remaining compared to the no-flow condition. Through this view, the significant difference between the different samples can be better illustrated. As shown in Fig. 9, it is again clear silicon performed the worst in retaining bacteria under flow. Bacteria on carbon film were resilient to a bulk velocity of $1.05\,mm\,s^{-1}$, followed by a significant loss at increased flow rates. The carbon nanofibers oriented perpendicular to the flow direction performed best in retaining bacteria under all flow rates tested, with 60% still on the surface even at the highest bulk velocity. Both randomly and parallel oriented nanofibers performed well at the intermediate bulk velocities, and while parallel fibers out-performed the carbon film at $3.15\,mm\,s^{-1}$, significant loss was observed at this flow rate. One hypothesis as to why perpendicularly oriented carbon nanofibers outperform the other carbon nanofiber orientations might be, that bacteria adhering to fibers with orientation perpendicular to flow have non-zero probability of experiencing reduced flow forces. The bacteria are most likely protected against flow by the fiber, or supported against flow force. Bacteria adhering to fibers oriented parallel to the flow direction likely do not enjoy such protection and are exposed directly to the flow force, although potentially with a smaller cross-section.

Bacteria adhesion-enabling behavior is dependent on different material and surface properties, such as wettability, the topography of the material in relation to bacteria size, material stiffness, and surface roughness [39]. The detected contact angle measurements correlate with the initial bacteria adhesion at $0\,mm\,s^{-1}$ for the carbon film and silicon samples. As discussed by Zheng et al. [39], wettability has a strong influence on bacteria adhesion, and hydrophilicity facilitates bacteria adhesion. The adhesion test results for the samples without carbon nanofibers indicate that the wettability is mainly relevant for the initial bacteria adhesion on smooth surfaces. This correlates with the detected bacteria amount at $0\,mm\,s^{-1}$. Carbon film with a contact angle of 50° has the highest wettability of the tested samples and also the highest initial bacteria adhesion with an approximate average of 69 counted bacteria per captured image and sample under no-flow conditions. Silicon had an average of 51 counted initial adhering bacteria under non-flow conditions and the second smallest contact angle of 59°. However, while the randomly oriented carbon nanofibers have the largest contact angle (99°), they had the second highest average of initial adhering bacteria counted of 67. Perpendicular fibers had an initial adhering bacteria amount of 25 and parallel aligned carbon nanofibers had 19. The different topography of the carbon nanofibers possibly influenced the initial adhesion of bacteria, hence, the wettability might not be the primary influence for the nanofiber samples. Due to the fibers having a diameter in the range of below 200 nm and *E. coli* having a length of 3 μm and diameter of 500 nm, the fiber size might impede the bacteria adhesion. Silicon has a flat surface, and carbon film is relatively flat as well, which might facilitate bacteria adhesion. Surface stiffness is another potential factor for cell adhesion, but previous studies were not conclusive and indicated that the bacteria size additionally needs to be investigated in this context [39]. Higher surface roughness enables increased bacteria adhesion and biofilm formation [39]. The surface roughness measurements of the samples showed that the carbon fiber samples have higher surface roughness than the carbon film and the silicon samples. This is a potential explanation for the bacteria density under flow conditions on the carbon nanofiber samples decreasing less then the smooth samples. Another factor might be the roughness of carbon nanofibers being similar to extracellular matrix material, which the bacteria might sense and hence attach in larger amounts.

Another possibility could be the random distribution of pore sizes for the randomly orientated carbon nanofibers, which offers the option of pores in the size of a bacterium and trapping bacteria in these pores. Additionally, carbon film has a higher surface roughness than silicon and reduced bacteria loss with increasing flow rate compared to silicon. Fig. 8 shows exemplary pictures of the fluorescence images of the different sample types at 0 and $3.15\,\mathrm{mm\,s^{-1}}$. The larger gaps between bacteria in the CF samples is likely caused by an uneven distribution of fibers. The images demonstrate the adhering bacteria have no orientational preference, regardless of the orientation of the carbon nanofibers. The fluorescence pictures of $3.15\,\mathrm{mm\,s^{-1}}$ further prove that the bacteria orientation does not change with flow applied. This indicates a strong adhesion of the bacteria to the sample surfaces.

Kallas et al. [52] applied a similar adhesion testing method to investigate the influence of Type 1 Fimbriae of *E. coli* on the bacterial adhesion to nanotstructured surfaces with 40 nm diameter pillars in polycarbonate with different surface coverage. However, they evaluated the results over the surface coverage of the bacteria and had a flow rate of $20\,\mathrm{mL\,min^{-1}}$ for 5 min. The results showed a clear trend of bacteria better adhering under these conditions with a higher nanostructure density. Nevertheless, different nanostructure shapes or sizes can potentially cause cell damage [52]. We observed a similar behavior, that the carbon nanofibers as nanostructures enabled better bacterial adhesion under flow conditions. Even better adhesion might be achieved with a denser fiber distribution and potentially oxygen plasma treatment of the fibers for increased wettability and thus higher initial bacteria adhesion. Investigation of the adhesive behavior of *E. coli* for higher flow conditions, like the one investigated by Kallas et al. [52] might be interesting in the future when the carbon nanofibers are utilized to different applications where a fast liquid exchange is necessary and the carbon nanofibers perform better than silicon or carbon film. Potential applications of those could be whole-cell biosensors on a MEMS device, to test toxicity or the presence of certain chemical compounds in mixing devices as well as the need for fast nutrition exchange.

4. Conclusions

In this study, bacterial adhesion on carbon nanofibers with different orientations, under flow conditions, was investigated. For further comparison, carbon film and silicon substrates were examined with regard to their ability to promote and sustain bacterial adhesion under the same flow conditions. The results for carbon nanofibers showed promising opportunities for adhesion under flow, even for higher flow rates used in this study. Compared with silicon and carbon film, the carbon nanofibers offered better support for the bacteria. Further, when the fibres were oriented perpendicularly to the flow, the best support for adhesion was found.

The outlook of this study, for the case of carbon nanofibers as a suitable matrix for hosting bacterial cells, is highly promising towards developing novel biohybrid living systems. However, more extensive investigations are required to fully clarify the interaction between bacteria and the carbon nanofiber substrate. Such fiber-based biohybrid systems could exhibit enhanced functionalities for different applications, due to the synergistic properties of the involved counterparts. Such applications might include living sensors for healthcare, sensors for environmental monitoring in harsh environments owing to the extremophilic behavior of certain bacteria and the compatibility of carbon, or for photosynthetic energy conversion which, in the future, may be useful for space exploration.

CRediT authorship contribution statement

Julia Schulte-Hermann: Writing – review & editing, Writing – original draft, Methodology, Investigation, Formal analysis, Conceptualization. **Hagen Rießland:** Writing – review & editing, Methodology, Investigation. **Stefan Hengsbach:** Writing – review & editing, Methodology, Investigation. **Jan G. Korvink:** Writing – review & editing, Funding acquisition. **Neil MacKinnon:** Writing – review & editing, Supervision, Funding acquisition, Formal analysis, Conceptualization. **Monsur Islam:** Writing – review & editing, Writing – original draft, Supervision, Investigation.

Declaration of competing interest

The authors declare that they have no known competing financial interests or personal relationships that could have appeared to influence the work reported in this paper.

Acknowledgments

The authors would like to acknowledge Richard Thelen for the surface characterization measurements. Dr. Georges Saliba is acknowledged for stimulating discussions on fluid dynamics. J.S-H., H.R., and N.M. were supported by the DFG under contract MA 6653/3-1. J.S-H., H.R., S.H., N.M., and J.G.K. acknowledge partial support from CRC 1527 *HyPERiON*. J.G.K. acknowledges partial support from the ERC-SyG (*HiSCORE*, 951459). The authors acknowledge the support of the Helmholtz Society through the program *Materials Systems Engineering*. M.I. and J.G.K acknowledge support from the DFG Cluster of Excellence *3D matter made to order*. M.I. also acknowledges partial support from the Deutsche Forschungsgemeinschaft (DFG, German Research Foundation) through project number 520292466 (Project title: *CeraLiFE*). The authors further acknowledge the support of the Karlsruhe Nano Micro Facility (KNMFi), a Helmholtz Research Infrastructure at Karlsruhe Institute of Technology.

Data availability

Data will be made available on request.

References

[1] S. Belkin, Microbial whole-cell sensing systems of environmental pollutants, Curr. Opin. Microbiol. 6 (3) (2003) 206–212, http://dx.doi.org/10.1016/S1369-5274(03)00059-6.
[2] S.J. Sørensen, M. Burmølle, L.H. Hansen, Making bio-sense of toxicity: new developments in whole-cell biosensors, Curr. Opin. Biotechnol. 17 (1) (2006) 11–16, http://dx.doi.org/10.1016/J.COPBIO.2005.12.007.
[3] D.M. Close, S. Ripp, G.S. Sayler, Reporter proteins in whole-cell optical bioreporter detection systems, biosensor integrations, and biosensing applications, Sensors (Basel, Switzerland) 9 (11) (2009) 9147, http://dx.doi.org/10.3390/S91109147.
[4] A.E. Zoheir, M.S. Sobol, D. Ordoñez-Rueda, A.-K. Kaster, C.M. Niemeyer, K.S. Rabe, A genetically-encoded three-colour stress biosensor reveals multimodal response at single cell level and spatiotemporal dynamics of biofilms, 2022, http://dx.doi.org/10.1101/2022.09.23.509207, bioRxiv 2022.09.23.509207.
[5] M.F. Moradali, B.H. Rehm, Bacterial biopolymers: from pathogenesis to advanced materials, Nat. Rev. Microbiol. 18 (4) (2020) 195–210, http://dx.doi.org/10.1038/s41579-019-0313-3.
[6] B.H. Rehm, Bacterial polymers: biosynthesis, modifications and applications, Nat. Rev. Microbiol. 8 (8) (2010) 578–592, http://dx.doi.org/10.1038/nrmicro2354.
[7] P. Anbu, C.H. Kang, Y.J. Shin, J.S. So, Formations of calcium carbonate minerals by bacteria and its multiple applications, SpringerPlus 5 (1) (2016) 1–26, http://dx.doi.org/10.1186/S40064-016-1869-2.
[8] B.E. Logan, J.M. Regan, Electricity-producing bacterial communities in microbial fuel cells, Trends Microbiol. 14 (12) (2006) 512–518, http://dx.doi.org/10.1016/j.tim.2006.10.003.
[9] D.P. Strik, H.V. Hamelers, J.F. Snel, C.J. Buisman, Green electricity production with living plants and bacteria in a fuel cell, Int. J. Energy Res. 32 (9) (2008) 870–876, http://dx.doi.org/10.1002/ER.1397.
[10] R. Sano, K. Koyama, N. Fukuoka, H. Ueno, S. Yamamura, T. Suzuki, Single-cell microarray chip with inverse-tapered wells to maintain high ratio of cell trapping, Micromachines 14 (2) (2023) 492, http://dx.doi.org/10.3390/MI14020492/S1.
[11] O. Peric, M. Hannebelle, J.D. Adams, G.E. Fantner, Microfluidic bacterial traps for simultaneous fluorescence and atomic force microscopy, Nano Res. 10 (11) (2017) 3896–3908, http://dx.doi.org/10.1007/S12274-017-1604-5/METRICS.

[12] A. Benavente-Babace, D. Gallego-Pérez, D.J. Hansford, S. Arana, E. Pérez-Lorenzo, M. Mujika, Single-cell trapping and selective treatment via co-flow within a microfluidic platform, Biosens. Bioelectron. 61 (2014) 298–305, http://dx.doi.org/10.1016/J.BIOS.2014.05.036.

[13] T. Braschler, R. Johann, M. Heule, L. Metref, P. Renaud, Gentle cell trapping and release on a microfluidic chip by in situ alginate hydrogel formation, Lab Chip 5 (5) (2005) 553–559, http://dx.doi.org/10.1039/B417604A.

[14] T. Bhattacharjee, S.S. Datta, Bacterial hopping and trapping in porous media, Nature Commun. 10 (1) (2019) http://dx.doi.org/10.1038/S41467-019-10115-1.

[15] J.R. Premkumar, O. Lev, R.S. Marks, B. Polyak, R. Rosen, S. Belkin, Antibody-based immobilization of bioluminescent bacterial sensor cells, Talanta 55 (5) (2001) 1029–1038, http://dx.doi.org/10.1016/S0039-9140(01)00533-1.

[16] I. Mani Pujitha, M. Khandelwal, C. Shekhar Sharma -, D. Svechkarev, M.R. Sadykov, L.J. Houser, W. Salalha, J. Kuhn, Y. Dror, E. Zussman, Encapsulation of bacteria and viruses in electrospun nanofibres, Nanotechnology 17 (18) (2006) 4675, http://dx.doi.org/10.1088/0957-4484/17/18/025.

[17] Y.F. Chu, C.H. Hsu, P.K. Soma, Y.M. Lo, Immobilization of bioluminescent Escherichia coli cells using natural and artificial fibers treated with polyethyleneimine, Bioresour. Technol. 100 (13) (2009) 3167–3174, http://dx.doi.org/10.1016/J.BIORTECH.2009.01.072.

[18] J. Schulte-Hermann, H. Rießland, N. MacKinnon, J.G. Korvink, M. Islam, Biomineralization of electrospun bacteria-encapsulated fibers: A relevant step toward living ceramic fibers, ACS Appl. Bio Mater. http://dx.doi.org/10.1021/acsabm.4c00715, PMID: 39205657.

[19] L.A.N. Julius, H. Scheidt, G. Krishnan, M. Becker, O. Nassar, S.M. Torres-Delgado, D. Mager, V. Badilita, J.G. Korvink, Dynamic dielectrophoretic cell manipulation is enabled by an innovative electronics platform, Biosens. Bioelectron.: X 14 (2023) 100333, http://dx.doi.org/10.1016/J.BIOSX.2023.100333.

[20] L. Zhu, M. Rajendram, K.C. Huang, Effects of fixation on bacterial cellular dimensions and integrity, iScience 24 (4) (2021) 102348, http://dx.doi.org/10.1016/j.isci.2021.102348.

[21] Q. Luan, C. Macaraniag, J. Zhou, I. Papautsky, Microfluidic systems for hydrodynamic trapping of cells and clusters, Biomicrofluidics 14 (3) (2020) 31502, http://dx.doi.org/10.1063/5.0002866.

[22] R.S. Shetty, S. Ramanathan, I.H. Badr, J.L. Wolford, S. Daunert, Green fluorescent protein in the design of a living biosensing system for L-arabinose, Anal. Chem. 71 (4) (1999) 763–768, http://dx.doi.org/10.1021/AC9811928/ASSET/IMAGES/LARGE/AC9811928F00005.JPEG.

[23] M. Yang, C.W. Li, J. Yang, Cell docking and on-chip monitoring of cellular reactions with a controlled concentration gradient on a microfluidic device, Anal. Chem. 74 (16) (2002) 3991–4001, http://dx.doi.org/10.1021/AC025536C/SUPPL_FILE/AC025536C.AVI.

[24] M.C. Flickinger, J.L. Schottel, D.R. Bond, A. Aksan, L.E. Scriven, Painting and printing living bacteria: Engineering nanoporous biocatalytic coatings to preserve microbial viability and intensify reactivity, Biotechnol. Prog. 23 (1) (2007) 2–17, http://dx.doi.org/10.1021/BP060347R.

[25] W. Xu, Biocompatibility and medical application of carbon material, Key Eng. Mater. 452–453 (2011) 477–480, http://dx.doi.org/10.4028/WWW.SCIENTIFIC.NET/KEM.452-453.477.

[26] S.K. Smart, A.I. Cassady, G.Q. Lu, D.J. Martin, The biocompatibility of carbon nanotubes, Carbon 44 (6) (2006) 1034–1047, http://dx.doi.org/10.1016/J.CARBON.2005.10.011.

[27] R. Petersen, Carbon fiber biocompatibility for implants, Fibers (Basel, Switzerland) 4 (1) (2016) http://dx.doi.org/10.3390/FIB4010001.

[28] Y.M. Eggeler, K.C. Chan, Q. Sun, A.D. Lantada, D. Mager, R. Schwaiger, P. Gumbsch, R. Schröder, W. Wenzel, J.G. Korvink, et al., A review on 3D architected pyrolytic carbon produced by additive micro/nanomanufacturing, Adv. Funct. Mater. (2023) 2302068.

[29] M. Islam, A. Sadaf, M.R. Gómez, D. Mager, J.G. Korvink, A.D. Lantada, Carbon fiber/microlattice 3D hybrid architecture as multi-scale scaffold for tissue engineering, Mater. Sci. Eng.: C 126 (2021) 112140, http://dx.doi.org/10.1016/J.MSEC.2021.112140.

[30] M. Islam, A. Díaz Lantada, D. Mager, J.G. Korvink, M. Islam, D. Mager, J.G. Korvink, A.D. Lantada, Carbon-based materials for articular tissue engineering: From innovative scaffolding materials toward engineered living carbon, Adv. Healthc. Mater. 11 (1) (2022) 2101834, http://dx.doi.org/10.1002/ADHM.202101834.

[31] E. Fuhrer, A. Bäcker, S. Kraft, F.J. Gruhl, M. Kirsch, N. MacKinnon, J.G. Korvink, 3D carbon scaffolds for neural stem cell culture and magnetic resonance imaging, Adv. Healthc. Mater. 7 (4) (2018) 1700915, http://dx.doi.org/10.1002/ADHM.201700915.

[32] A. Mohammadpour-Haratbar, S. Mohammadpour-Haratbar, Y. Zare, K.Y. Rhee, S.-J. Park, A review on non-enzymatic electrochemical biosensors of glucose using carbon nanofiber nanocomposites, Biosensors 12 (11) (2022) 1004.

[33] Z. Wang, S. Wu, J. Wang, A. Yu, G. Wei, Carbon nanofiber-based functional nanomaterials for sensor applications, Nanomaterials 9 (7) (2019) 1045.

[34] Z. Lu, R. Raad, F. Safaei, J. Xi, Z. Liu, J. Foroughi, Carbon nanotube based fiber supercapacitor as wearable energy storage, Front. Mater. 6 (2019) 138.

[35] S. Chen, L. Qiu, H.-M. Cheng, Carbon-based fibers for advanced electrochemical energy storage devices, Chem. Rev. 120 (5) (2020) 2811–2878.

[36] M. Islam, C. Selhuber-Unkel, J.G. Korvink, A.D. Lantada, Engineered living carbon materials, Matter 6 (5) (2023) 1382–1403.

[37] M. Islam, P.G. Weidler, S. Heissler, D. Mager, J.G. Korvink, Facile template-free synthesis of multifunctional 3D cellular carbon from edible rice paper, RSC Adv. 10 (28) (2020) 16616–16628.

[38] R. Natu, M. Islam, R. Martinez-Duarte, Shrinkage analysis of carbon micro structures derived from SU-8 photoresist, ECS Trans. 72 (1) (2016) 27.

[39] S. Zheng, M. Bawazir, A. Dhall, H.E. Kim, L. He, J. Heo, G. Hwang, Implication of surface properties, bacterial motility, and hydrodynamic conditions on bacterial surface sensing and their initial adhesion, Front. Bioeng. Biotechnol. 9 (2021) 643722, http://dx.doi.org/10.3389/FBIOE.2021.643722/BIBTEX.

[40] K. Elfazazi, H. Zahir, S. Tankiouine, B. Mayoussi, C. Zanane, S. Lekchiri, M. Ellouali, E.M. Mliji, H. Latrache, Adhesion behavior of escherichia coli strains on glass: Role of cell surface qualitative and quantitative hydrophobicity in their attachment ability, Int. J. Microbiol. 2021 (2021) http://dx.doi.org/10.1155/2021/5580274.

[41] P. Buahom, Measuring the contact angle using imagej with contact angle plug-in, 2018, http://dx.doi.org/10.13140/RG.2.2.33978.85445/1.

[42] K.-Y. Law, Definitions for hydrophilicity, hydrophobicity, and superhydrophobicity: Getting the basics right, J. Phys. Chem. Lett. 5 (4) (2014) 686–688, http://dx.doi.org/10.1021/jz402762h, PMID: 26270837.

[43] G. Udupa, M. Singaperumal, R.S. Sirohi, M.P. Kothiyal, Characterization of surface topography by confocal microscopy: I. principles and the measurement system, Meas. Sci. Technol. 11 (2000) 305, http://dx.doi.org/10.1088/0957-0233/11/3/320.

[44] Keyence Corporation, Sa (Arithmetical Mean Height), https://www.keyence.com/ss/products/microscope/roughness/surface/parameters.jsp.

[45] Keyence Corporation, Sq (Root Mean Square Height), https://www.keyence.com/ss/products/microscope/roughness/surface/sq-root-mean-square-height.jsp.

[46] T. Peschke, K.S. Rabe, C.M. Niemeyer, Orthogonal surface tags for whole-cell biocatalysis, Angew. Chem., Int. Ed. Engl. 56 (8) (2017) 2183–2186, http://dx.doi.org/10.1002/ANIE.201609590.

[47] C.H. Liao, L.M. Shollenberger, Survivability and long-term preservation of bacteria in water and in phosphate-buffered saline, Lett. Appl. Microbiol. 37 (1) (2003) 45–50, http://dx.doi.org/10.1046/j.1472-765X.2003.01345.x.

[48] N.C. Martin, A.A. Pirie, L.V. Ford, C.L. Callaghan, K. McTurk, D. Lucy, D.G. Scrimger, The use of phosphate buffered saline for the recovery of cells and spermatozoa from swabs, Sci. Justice 46 (3) (2006) 179–184, http://dx.doi.org/10.1016/S1355-0306(06)71591-X.

[49] S.W.M.A.I. Senevirathne, A. Mathew, Y.-C. Toh, P.K.D.V. Yarlagadda, Bactericidal efficacy of nanostructured surfaces increases under flow conditions, ACS Omega 7 (45) (2022) 41711–41722, http://dx.doi.org/10.1021/acsomega.2c05828.

[50] S. Berg, D. Kutra, T. Kroeger, C.N. Straehle, B.X. Kausler, C. Haubold, M. Schiegg, J. Ales, T. Beier, M. Rudy, K. Eren, J.I. Cervantes, B. Xu, F. Beuttenmueller, A. Wolny, C. Zhang, U. Koethe, F.A. Hamprecht, A. Kreshuk, ilastik: interactive machine learning for (bio)image analysis, Nat. Methods (2019) http://dx.doi.org/10.1038/s41592-019-0582-9.

[51] M. Kim, Y. Kim, K.M. Lee, S.Y. Jeong, E. Lee, S.H. Baeck, S.E. Shim, Electrochemical improvement due to alignment of carbon nanofibers fabricated by electrospinning as an electrode for supercapacitor, Carbon 99 (2016) 607–618.

[52] P. Kallas, H.J. Haugen, N. Gadegaard, J. Stormonth-Darling, M. Hulander, M. Andersson, H. Valen, Adhesion of escherichia coli to nanostructured surfaces and the role of type 1 fimbriae, Nanomaterials 10 (11) (2020) 1–13, http://dx.doi.org/10.3390/nano10112247.